Antichiral Edge States in a Modified Haldane Nanoribbon

E. Colomés[1,2,*] and M. Franz[2,†]

[1]*Departament d'Enginyeria Electrònica, Universitat Autònoma de Barcelona, 08193-Bellaterra (Barcelona), Spain*
[2]*Department of Physics and Astronomy and Quantum Matter Institute, University of British Columbia, Vancouver, British Columbia, Canada V6T 1Z4*

Topological phases of fermions in two dimensions are often characterized by chiral edge states. By definition, these propagate in opposite directions at the two parallel edges when the sample geometry is that of a rectangular strip. We introduce here a model which exhibits what we call "antichiral" edge modes. These propagate *in the same direction* at both parallel edges of the strip and are compensated by counterpropagating modes that reside in the bulk. General arguments and numerical simulations show that backscattering is suppressed even when strong disorder is present in the system. We propose a feasible experimental realization of a system showing such antichiral edge modes in transition metal dichalcogenide monolayers.

Introduction.—Topologically protected edge states in two-dimensional (2D) fermionic systems occur in two common varieties. *Chiral* edge modes are found in systems with broken time-reversal symmetry such as the quantum Hall or Haldane insulators [1,2]. In a strip geometry, the bulk is gapped and the protected edge modes are counterpropagating as illustrated in Fig. 1(a). *Helical* edge modes occur in time-reversal-invariant systems, such as the 2D quantum spin Hall effect (QSHE) [3,4], and can be regarded as two superimposed copies of Haldane insulators related by time-reversal symmetry. In this case, the bulk is also gapped, and each edge contains a pair of counterpropagating spin filtered states illustrated in Fig. 1(b). In both cases, backscattering is suppressed exponentially with the width W of the strip and leads to effectively dissipationless edge transport in the limit of large W [5]. Such loss-free transport has obvious technological potential and underlies much of the current interest in topological states of matter.

In this Letter, we ask the following question: Is it possible to have a 2D fermionic system with copropagating edge modes, illustrated in Fig. 1(c)? A simple consideration shows that such "antichiral" edge modes cannot exist in a system with a full bulk gap. This is because the number of left- and right-moving modes in any finite system defined on the lattice must be the same. Only then can one define a legitimate band structure with full Brillouin zone periodicity. We show, however, that antichiral edge modes indeed can exist in 2D semimetals, where gapless bulk states supply the required counterpropagating modes. The edge modes are still topologically protected, much like Fermi arcs in 3D Dirac and Weyl semimetals [6,7]. They also carry nearly dissipationless currents, although the exponential protection against backscattering is replaced by a

power law due to the extended nature of the counterpropagating bulk modes.

A similar situation has been encountered recently [8–10] in a 3D Weyl semimetal wire, where the energy dispersion is modified such that conducting surface modes propagate in one direction only and bulk modes propagate in the other. In such a "topological coaxial cable," backscattering is strongly suppressed, because bulk and surface modes are spatially separated. Reliable numerical simulations of this system with disorder are, however, quite challenging owing to its 3D nature. Here we construct a 2D system with analogous physical properties in which numerical results can be obtained up to very large sizes.
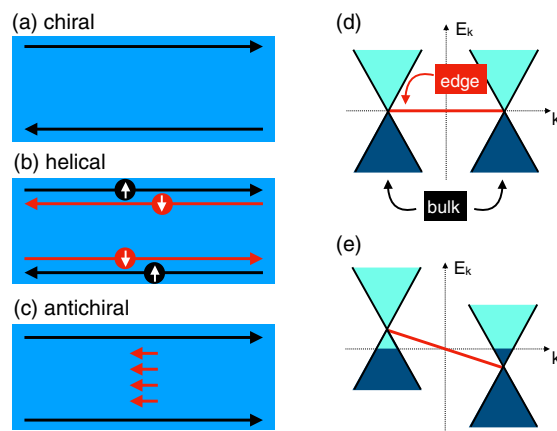

FIG. 1. Schematic of a topological state with (a) chiral, (b) helical, and (c) antichiral edge modes. Panel (d) illustrates the low-energy dispersion of a zigzag graphene nanoribbon with a dispersionless edge state (red) connecting two Dirac points. Applying the pseudoscalar potential in (e) offsets the Dirac points in energy and causes the edge mode to disperse.

A system we consider in this Letter takes inspiration from a graphene nanoribbon with zigzag edges [11]. It is well known that such a nanoribbon exhibits dispersionless edge states—zero-energy flat bands—that span projections of two inequivalent Dirac points onto the 1D Brillouin zone characterizing the ribbon [12–14] [Fig. 1(d)]. These edge modes are topologically protected in a similar way as the Fermi arcs in 3D Dirac and Weyl semimetals [15–17]. The key idea is to add a pseudoscalar potential term to the Hamiltonian H_0 describing such a ribbon so that the two Dirac points are shifted in energy in the *opposite* direction. As a result, the edge modes acquire a dispersion [Fig. 1(e)], which is now, crucially, the same for both edges. We thus obtain a system with two copropagating edge modes compensated by counterpropagating bulk modes. Mathematically, the requisite pseudoscalar potential follows from a term that is similar to the Haldane mass [2] for spinless fermions and describes a second-neighbor complex hopping between sites. We show that a variant of such a term is actually realized in transition metal dichalcogenide monolayers when one includes spin.

Modified Haldane model.—We seek a term to add to the graphene Hamiltonian which breaks time-reversal symmetry ($\mathcal{T}$) and acts as a scalar potential with an opposite sign in each valley. In 1988, Haldane [2] introduced a model realizing quantized Hall conductance without an external magnetic field, defined by the Hamiltonian

$$H = t_1 \sum_{\langle i,j \rangle} c_i^\dagger c_j + t_2 \sum_{\langle\langle i,j \rangle\rangle} e^{-iv_{ij}\phi} c_i^\dagger c_j, \quad (1)$$

where c_i is an annihilation operator for a spinless fermion on site $\boldsymbol{R}_i$ of the honeycomb lattice. The next-nearest-neighbor (NNN) hopping breaks the $\mathcal{T}$ symmetry due to the phase ϕ and is different when it links two A atoms or B atoms [$v_{ij} = \pm 1$; see also the inset in Fig. 2(a)]. In the continuum theory, the Hamiltonian can be rewritten as

$$H = \hbar v_F (\sigma_x \tau_z q_x + \sigma_y \tau_0 q_y) + t_2^a \sigma_z \tau_z + t_2^b \sigma_0 \tau_0, \quad (2)$$

where v_F is the Fermi velocity, $\boldsymbol{\sigma}$ and $\boldsymbol{\tau}$ are the Pauli matrices acting in the sublattice and valley spaces, respectively, and $\boldsymbol{q}$ is the momentum relative to the Dirac points. In addition, $t_2^a = -3\sqrt{3}t_2 \sin\phi$, and $t_2^b = -3t_2 \cos\phi$. In Fig. 2(a), we display the band structure of the Haldane nanoribbon. When the Fermi energy E_F lies close to zero energy, it crosses the two edge states which connect the two Dirac points. One edge mode is right moving and the other left moving as expected of the chiral edge modes.

Importantly for our goal of constructing a pseudoscalar perturbation, we observe in Eq. (2) that the Haldane term $t_2^a \sigma_z \tau_z$ anticommutes with the rest of the Hamiltonian and acts therefore as a mass term. If we were to modify this term to act equally in both sublattices (i.e., replacing $\sigma_z \to \sigma_0$), then it would commute with the rest of the Hamiltonian and
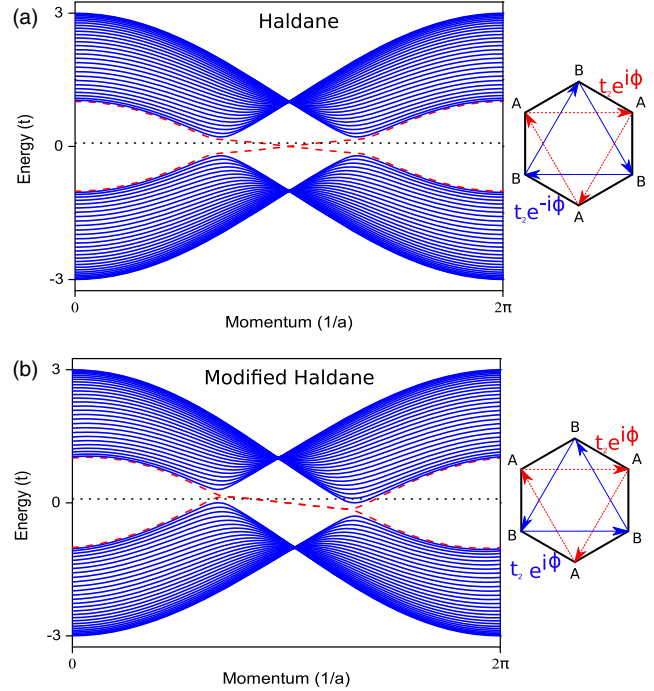

FIG. 2. Band structure of a zigzag nanoribbon (ZGNR) of width $W = 60$ (60 ZGNR) described by the (a) Haldane and (b) modified Haldane Hamiltonian. t_1 is taken as the unit of energy, $t_2 = 0.03$, and $\phi = \pi/2$. The insets show the pattern of phases for the NNN hopping terms.

play the role of a pseudoscalar potential instead. On the lattice, this can be achieved if we make the NNN hopping term to act equally in both A and B sublattices; i.e., in Eq. (1), we set $v_{ij} = +1$ for all sites [see the inset in Fig. 2(a)]. With this change, the "modified Haldane model" (MHM) at low energies becomes

$$H = \hbar v_F (\sigma_x \tau_z q_x + \sigma_y \tau_0 q_y) + t_2^a \sigma_0 \tau_z + t_2^b \sigma_0 \tau_0. \quad (3)$$

The excitation spectrum reads

$$E_{\boldsymbol{q}} = \pm \hbar v_F \sqrt{q_x^2 + q_y^2} + t_2^a \tau_z + t_2^b, \quad (4)$$

showing that the two Dirac points are indeed offset in energy by $\pm t_2^a$ as outlined in Fig. 1(e). On the basis of arguments presented in the introduction, we expect that the MHM should exhibit antichiral edge modes.

In Fig. 2(b), we display the band structure of the MHM. The Dirac points are shifted in energy, and the edge modes acquire dispersion with the same velocity; i.e., both edge modes propagate in the same direction. We see also that the Fermi energy crosses bulk modes, as it should because the total number of left- and right-moving modes must be the same. The important point is that these modes belong to the bulk and are therefore spatially separated from the edge modes. We therefore expect backscattering of the edge

modes to be strongly suppressed. An electron in the edge that suffers a collision with an impurity cannot backscatter unless it moves to the bulk.

Results.—In pristine graphene, the zigzag edge zero modes are protected by the chiral symmetry $\mathcal{C}$: $\sigma_z H_0 \sigma_z = -H_0$, which allows a topological winding number to be defined [15,16]. We review this topological protection in Supplemental Material [18] and show that it applies to the modified Haldane model as well. In essence, because the MHM term is proportional to the unit matrix in the sublattice space, it does not modify the spinor structure of the wave functions compared to the pristine case (although it does change their energies). Since the topology is encoded in the wave functions, we expect the edge modes to persist, except that they may now occur away from zero energy. This indeed is seen in Fig. 2(b).

To demonstrate the extreme robustness of the antichiral edge modes in the MHM against disorder, we compute [23,24] the conductance G as a function of the length L of the ribbon for different impurity concentrations n_I. We consider a system depicted in Fig. 3(a), where the black part corresponds to the active region with disorder and the red part represents the contacts. Impurities are introduced as on-site potentials, whose energy value is randomly chosen in the interval $[-U, U]$. Simulations are repeated for different impurity configurations, and the conductance is averaged over these. Impurity concentration n_I is expressed as the number of defected sites divided by the total number of atoms in the system.

In Fig. 3(b), we plot the conductance as a function of the length of the ribbon. For a clean sample ($n_I = 0$), the conductance (in units of e^2/h) equals to 4, independently of the length of the system. This can be explained by noting that for the adopted parameters E_F crosses two right-moving bulk modes in addition to two right-moving edge modes. When disorder is introduced, we observe an initial fast drop in conductance with L. We interpret this as Anderson localization [25,26] of the bulk modes. However, contrary to the ordinary zigzag nanoribbon, where the conductance drops to zero [27], in the MHM the conductance reaches the value of 2 and then remains essentially constant even for very long ribbons and very high values of disorder. This occurs because two edge modes (and two counterpropagating bulk modes) remain delocalized and continue exhibiting ballistic transport. We emphasize that these modes are extremely robust. For instance, for $n_I = 0.6$ corresponding to very strong disorder with 60% of sites containing defects (far higher than disorder levels in realistic graphene samples [14]) and $L = 1500$, the conductance decreases only by about 5%.

These results suggest that the MHM can be characterized by two localization lengths, one for the bulk modes, which we define as $\lambda_b^{-1} = d \ln(G - 2)/dL|_{L < \lambda_b}$, and one for the edge modes, $\lambda_e^{-1} = d \ln(G)/dL|_{L > \lambda_b}$. From Fig. 3(b), we can estimate both localization lengths. We find that values
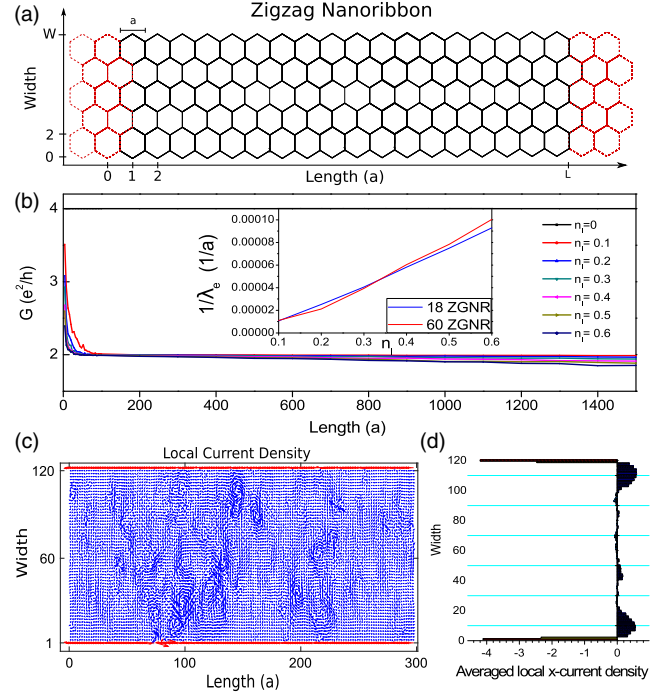

FIG. 3. (a) Zigzag nanoribbon structure used in the numerical simulations. (b) Conductance as a function of L for $W = 60$, $U = 2.5$, and E_F set close to zero. Different disorder concentrations are depicted. Inset: Inverse edge state localization length λ_e estimated from the decay in conductance $G(L) \simeq 2(1 - L/\lambda_e)$ in the regime $\lambda_b \ll L \ll \lambda_e$. We checked that the conductance is the same when the current flows from left to right and vice versa, as required by conductance reciprocity. (c) Local current density (LCD) of a 120 ZGNR and $L = 300$ for E_F close to zero when $n_I = 0.1$. (d) Average of the LCD in the x direction of (c) as a function of the width of the ribbon.

obtained for λ_b are similar to localization length results found in the literature for similar systems [27], while λ_e is much longer, expressing the fact that the edge modes are extremely difficult to localize.

To elucidate the anomalously long localization length of the edge states, we performed some analytical calculations. We expect these edge states to exponentially decay into the bulk, with the wave function of the form $\psi_e(\mathbf{r}) \simeq e^{ikx - y/\xi}/\sqrt{\xi L}$. If we assume that the counterpropagating bulk states are roughly constant throughout the sample with $\psi_b(\mathbf{r}) \simeq e^{-ikx}/\sqrt{WL}$, it is easy to obtain an expression for the elastic scattering rate $\hbar/\tau = n_I(\xi a^4 u_0^2/2 v \hbar W^2)$. Here a is the lattice constant, u_0 is the average impurity potential strength, v is the velocity, and ξ is the typical decay length for the edge states. The localization length in one dimension is $\lambda_e = \pi l$, where $l = v\tau$ is the mean free path. We obtain

$$\lambda_e = \frac{2v^2 \hbar^2 W^2 \pi}{n_I \xi a^4 u_0^2}. \tag{5}$$

The inset in Fig. 3(b) confirms the expected dependence of λ_e on the impurity concentration n_I. The expected dependence on width W is, however, not borne out; we find that the last remaining counterpropagating bulk states are not fully extended over the width of the sample but are instead concentrated along the edges with a characteristic length scale $\xi' \gg \xi$. This is illustrated in Figs. 3(c) and 3(d). The expression Eq. (5) thus holds if we replace $W \to \xi'$, producing a long localization length, which, however, does not diverge in the limit of a wide strip. At present, we do not fully understand the origin of the length scale ξ', but we note that it may herald interesting new physics in systems with antichiral edge modes to be explored in future studies.

Proposed experimental realizations.—The direct experimental realization of our model faces the same challenges as the Haldane model, which has only recently been realized using ultracold atoms in an optical lattice [28]. The same method could be used to realize the modified Haldane model. We also note a recent proposal invoking an iron-based ferromagnetic insulator lattice [29].

Another route is based on the idea advanced by Kane and Mele [3], who noted that NNN tunneling amplitudes of the type required by the Haldane model can be supplied by spin-orbit coupling (SOC), creating effectively two copies of the HM for two projections of the electron spin, conjugate under $\mathcal{T}$. SOC is intrinsically very weak in graphene, but the QSHE was experimentally realized in HgTe quantum wells [30]. Our strategy, therefore, is to generalize the model to spinful fermions with SOC and obtain two copies of the MHM conjugate under $\mathcal{T}$. In contrast to the HM, our model intrinsically breaks the inversion symmetry; therefore, we have to include SOC in a noncentrosymmetric system. For that reason, hexagonal transition metal dichalcogenide (TMD) monolayers MX_2 are excellent candidates. In their monolayer form, the $M = W$, Mo atom is sandwiched between two $X = S$, Se, Te atoms with D_{3h}^1 crystal structure [31]. TMDs have a similar band structure to graphene, with two nonequivalent Dirac points in the corners of the Brillouin zone but with a band gap due to the hybridization of the d orbitals [32] and with stronger SOC, since they are composed of heavy elements [33]. Xiao *et al.* [34] proposed a low-energy Hamiltonian for these materials and predicted selection rules for optical interband transitions, which have been tested experimentally [35–37]. The Hamiltonian is

$$H = \hbar v_F (\sigma_x \tau_z q_x + \sigma_y \tau_0 q_y) - \lambda \tau_z \frac{\sigma_z - \sigma_0}{2} s_z + \sigma_z m_S, \quad (6)$$

where λ is the SOC parameter and s_z represents the spin. We observe that in each spin sector SOC produces the desired pseudoscalar term proportional to $\tau_z \sigma_0$ in addition to the Haldane term $\tau_z \sigma_z$ and the inversion symmetry-breaking "Semenoff mass" m_S. It is easy to construct the lattice version of Eq. (6) and compute the band structure. For the spin-up electrons, this is displayed in Fig. 4(a) (the
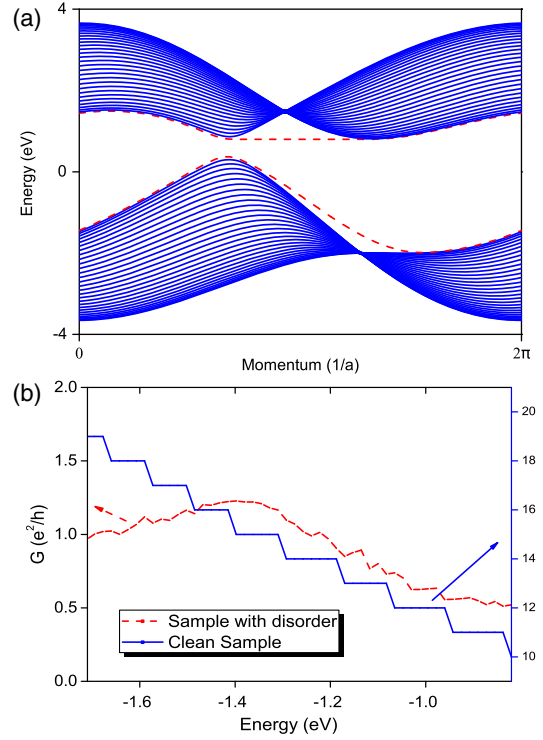

FIG. 4. (a) WSe$_2$ band structure for a 60 ZGNR and $L = 300$. Parameters used for the simulation are $t = 1.19$ eV, $m_S = 0.8$ eV, and $\lambda = 0.23$ eV. (b) Conductance for the interval of energies where the edge state exists in the valence band. The blue solid line corresponds to a clean sample, while the red dashed line to a system with $n_I = 0.1$.

spin-down band structure is the same but reversed in momentum around the origin of the BZ). For the simulation, we chose $M = W$ and $X = Se$, since WSe$_2$ has the strongest SOC of all TMD monolayers [38].

There are some obvious differences between Fig. 4(a) and the ideal MHM band structure in Fig. 2(b). Most importantly, WSe$_2$ exhibits a full bulk band gap, whereas the MHM remains gapless. Nevertheless, WSe$_2$ shows edge modes that may be regarded as descendants of those in the MHM. Indeed, it is easy to see that one can evolve the band structure in Fig. 2(b) into Fig. 4(a) by gradually turning on the Haldane and Semenoff mass parameters. This illustrates the robustness of the topological protection even with $\mathcal{C}$ strongly broken. If the Fermi energy crosses the WSe$_2$ edge mode in the valence band, similarly to our model, a current will flow along one edge of the sample with the countercurrent returning through the bulk. In this sense, the WSe$_2$ zigzag nanoribbon realizes the physics of the antichiral edge modes, and we expect them to be robust against disorder. Figure 4(b) shows the conductance as a function of E_F for WSe$_2$. We find that disorder quickly localizes all the bulk modes and only the edge mode survives, leading to conductance close to e^2/h. Interestingly, the edge currents in WSe$_2$ are spin polarized, which could be useful in spintronic applications.

Conclusions.—We discussed 2D systems where nearly dissipationless currents occur because left- and right-moving modes are segregated to the edges and the bulk of the sample, respectively. For that reason, backscattering is suppressed, even for samples with high impurity concentrations. A simple system showing this behavior can be constructed by slightly modifying the well-known Haldane model [2]. A variant of this model (for spinful fermions) is approximately realized in TMD monolayers and can be used to experimentally test the physics of antichiral edge modes.

---

[*]enrique.colomes@uab.es

[†]franz@phas.ubc.ca

[1] R. B. Laughlin, Phys. Rev. B **23**, 5632 (1981).

[2] F. D. M. Haldane, Phys. Rev. Lett. **61**, 2015 (1988).

[3] C. L. Kane and E. J. Mele, Phys. Rev. Lett. **95**, 226801 (2005).

[4] M. Z. Hasan and C. L. Kane, Rev. Mod. Phys. **82**, 3045 (2010).

[5] For helical edge states, unbroken time-reversal symmetry and negligible interaction strength must be maintained to achieve dissipationless transport.

[6] X. Wan, A. M. Turner, A. Vishwanath, and S. Y. Savrasov, Phys. Rev. B **83**, 205101 (2011).

[7] O. Vafek and A. Vishwanath, Annu. Rev. Condens. Matter Phys. **5**, 83 (2014).

[8] T. Schuster, T. Iadecola, C. Chamon, R. Jackiw, and S. Y. Pi, Phys. Rev. B **94**, 115110 (2016).

[9] D. I. Pikulin, A. Chen, and M. Franz, Phys. Rev. X **6**, 041021 (2016).

[10] P. Baireuther, J. A. Hutasoit, J. Tworzydo, and C. W. J. Beenakker, New J. Phys. **18**, 045009 (2016).

[11] A. K. Geim and K. S. Novoselov, Nat. Mater. **6**, 183 (2007).

[12] M. Fujita, K. Wakabayashi, K. Nakada, and K. Kusakabe, J. Phys. Soc. Jpn. **65**, 1920 (1996).

[13] K. Wakabayashi and M. Sigrist, Phys. Rev. Lett. **84**, 3390 (2000).

[14] A. H. Castro Neto, F. Guinea, N. M. R. Peres, K. S. Novoselov, and A. K. Geim, Rev. Mod. Phys. **81**, 109 (2009).

[15] S. Ryu and Y. Hatsugai, Phys. Rev. Lett. **89**, 077002 (2002).

[16] P. Delplace, D. Ullmo, and G. Montambaux, Phys. Rev. B **84**, 195452 (2011).

[17] M. Kharitonov, J.-B. Mayer, and E. M. Hankiewicz, Phys. Rev. Lett. **119**, 266402 (2017).

[18] See Supplemental Material at http://link.aps.org/supplemental/10.1103/PhysRevLett.120.086603 for clarifying the topological protection of the zigzag edges modes, which includes Refs. [15–17,19–22].

[19] A. Altland and M. R. Zirnbauer, Phys. Rev. B **55**, 1142 (1997).

[20] J. Zak, Phys. Rev. Lett. **62**, 2747 (1989).

[21] See, e.g., C. L. Kane, in *Topological Insulators*, edited by M. Franz and L. Molenkamp (Elsevier, Oxford, 2013).

[22] W. P. Su, J. R. Schrieffer, and A. J. Heeger, Phys. Rev. Lett. **42**, 1698 (1979).

[23] Numerical simulations were performed with the ᴋᴡᴀɴᴛ tight-binding code.

[24] C. W. Groth, M. Wimmer, A. R. Akhmerov, and X. Waintal, New J. Phys. **16**, 063065 (2014).

[25] A. Lagendijk, B. van Tiggelen, and D. S. Wiersma, Phys. Today **62**, No. 8, 24 (2009).

[26] P. W. Anderson, Phys. Rev. **109**, 1492 (1958).

[27] I. Kleftogiannis, I. Amanatidis, and V. A. Gopar, Phys. Rev. B **88**, 205414 (2013).

[28] G. Jotzu, M. Messer, R. Desbuquois, M. Lebrat, T. Uehlinger, D. Greif, and T Esslinger, Nature (London) **515**, 237 (2014).

[29] H. Kim and H. Kee, npj Quantum Mater. **2**, 20 (2017).

[30] M. König, S. Wiedmann, C. Brune, A. Roth, H. Buhmann, L. W. Molenkamp, X.-L. Qi, and S.-C. Zhang, Science **318**, 766 (2007).

[31] J. Ribeiro-Soares, R. M. Almeida, E. B. Barros, P. T. Araujo, M. S. Dresselhaus, L. G. Cancado, and A. Jorio, Phys. Rev. B **90**, 115438 (2014).

[32] L. F. Mattheiss, Phys. Rev. B **8**, 3719 (1973).

[33] J. A. Reyes-Retana and F. Cervantes-Sodi, Sci. Rep. **6**, 24093 (2016).

[34] D. Xiao, G. B. Liu, W. Feng, X. Xu, and W. Yao, Phys. Rev. Lett. **108**, 196802 (2012).

[35] K. F. Mak, K. He, J. Shan, and T. F. Heinz, Nat. Nanotechnol. **7**, 494 (2012).

[36] H. Zeng, J. Dai, W. Yao, D. Xiao, and X. Cui, Nat. Nanotechnol. **7**, 490 (2012).

[37] T. Cao, G. Wang, W. Han, H. Ye, C. Zhu, J. Shi, Q. Niu, P. Tan, E. Wang, B. Liu, and J. Feng, Nat. Commun. **3**, 887 (2012).

[38] Z. Y. Zhu, Y. C. Cheng, and U. Schwingenschlögl, Phys. Rev. B **84**, 153402 (2011).